ELSEVIER

Journal of Fluids and Structures 23 (2007) 23–37

JOURNAL OF FLUIDS AND STRUCTURES

www.elsevier.com/locate/jfs

Numerical simulation of vortex-induced vibration of a circular cylinder at low mass-damping using RANS code

Z.Y. Pan[a], W.C. Cui[b,*], Q.M. Miao[b]

[a]*State Key Laboratory of Ocean Engineering, Shanghai Jiao Tong University, Shanghai 200030, China*
[b]*China Ship Scientific Research Center, P.O. Box 116, Wuxi, Jiangsu 214082, China*

Received 15 November 2004; accepted 30 July 2006
Available online 25 September 2006

Abstract

Fundamental research on vortex-induced vibration (VIV) of a circular cylinder is still needed to build more rational VIV analysis tools for slender marine structures. Numerical results are presented for the response of an elastically mounted rigid cylinder at low mass damping constrained to oscillate transversely to a free stream. A two-dimensional Reynolds-averaged Navier–Stokes (RANS) code equipped with the SST $k-\omega$ turbulence model is applied for the numerical calculations. The numerical results are compared in detail with recent experimental and computational work. The Reynolds-averaging procedure erases the random disturbances in the vortex shedding process, so that the comparison between experimental data and the numerical results obtained by RANS codes may reveal some random characteristics of the VIV response. How random disturbance affects the observation in the experiments is discussed in this paper and the issues influencing the appearance of the upper branch in experiments are especially investigated. The absence of the upper branch in RANS simulations is explained in depth on account of discrepancies, which exist between experiments and RANS simulations. In addition, the formation of the 2P vortex shedding mode and its transition through the lock-in region are well reproduced in this investigation.

Keywords: Vortex-induced vibration (VIV); Circular cylinder; RANS; Vortex shedding mode

1. Introduction

Vortex-induced vibration (VIV) arises in many engineering areas, especially in coastal and marine applications such as marine cables, subsea pipelines and flexible risers. The increased interest in worldwide deep-water petroleum production draws renewed attention to research activities on VIV of slender marine risers; see recent overviews on VIV by Sarpkaya (2004) and Williamson and Govardhan (2004).

Analyses of VIVs of marine risers are performed either by empirical prediction tools which depend on experimental data, or by computational fluid dynamics (CFD) techniques in which the viscous Navier–Stokes equations are numerically solved to obtain the hydrodynamic forces directly. In empirical models, slender risers are usually divided into elements, so that one can use the data from measurements on rigid cylinders undergoing vortex-induced or forced vibrations. Correspondingly, CFD methods often cooperate with the strategy known as the "strip theory approach" in

*Corresponding author. Tel.: +86 510 8555 5660; fax: +86 510 8555 5193.
E-mail addresses: pzyss@sjtu.org (Z.Y. Pan), wccui@sjtu.edu.cn (W.C. Cui), qmmiao@yahoo.com (Q.M. Miao).

0889-9746/$ - see front matter
doi:10.1016/j.jfluidstructs.2006.07.007

which computations by 2-D CFD codes are carried out for a number of strips along the riser and loads are then applied to the structure for the dynamic analysis. Currently, large discrepancies exist between the results obtained by different prediction schemes due to different assumptions and experimental data-bases employed in empirical methods; on the other hand, due to uncertainties in CFD techniques over the modeling of the vortex-shedding interacting with dynamic response of the structure [see Larsen and Halse (1997) and Chaplin et al. (2005)]. Therefore, more fundamental research work on rigid cylinder sections, both experimental and computational, is still necessary in order to deepen our understanding on VIV of slender marine structures.

Recently, there have been many publications on VIV of an elastically mounted cylinder at low mass damping constrained to move transversely in a uniform incoming flow. Much progress has been made by Prof. Williamson's group with a series of physical experiments (Khalak and Williamson, 1996; Khalak and Williamson, 1999; Govardhan and Williamson, 2000). The main results can be summarized as follows. For a cylinder (of diameter D) with low mass ratio m^* (structure mass/displaced fluid mass) and damping ratio ζ, as the flow velocity U is varied (U is normalized by different researchers with the natural frequency of the structure in vacuum $U_r = U/f_nD$ or in water $U^* = U/f_{wtr}D$), three distinct response branches are observed with different response amplitude A; namely the *initial branch*, the *upper branch* and the *lower branch*. The upper branch is absent in the classical high mass-damping cases (Feng, 1968). The transition between the initial and upper branches is found to be hysteretic, while the transition from the upper to lower branch is assumed to be involved in an intermittent switching in response with a jump in phase ϕ (between the lift force and cylinder response) by about 180°. Amplitude modulation is observed in the initial branch, indicating a combination of two frequencies. In the upper and lower branches, the vortex-shedding frequency is locked on to the response frequency of the cylinder. The extent of such a synchronization region (measured by the range of U^*) is determined primarily by m^*. Moreover, it has been found in experimental work that there is a correspondence of the 2S mode (two single vortices shed per cycle) with the initial branch, and the 2P mode (two pair vortices shed per cycle) with the lower branch. The 2P mode is also observed in the upper branch, but the second vortex of each pair is much weaker than the first one.

However, the departure of the upper branch from the lower branch and the random characteristics of the response are not well understood. Moreover, few numerical studies have reported the 2P mode (Blackburn et al., 2001; Lucor et al., 2005), much less on the vortex-shedding mode transition through the lock-in region. The debate remains on the existence of the 2P mode as a steady-state pattern. Al Jamal and Dalton (2005) reviewed recent numerical studies on VIV of a circular cylinder and investigated the irregular behavior of the phase angle. Apparently, all vortex-shedding-related problems appear irregular in the vortex shedding mode, fluid forces and body response. Such an irregular phenomenon complicates the physical problem and handicaps our observations.

The span-wise correlation of the wake and then that of the fluid force remain hot issues. It is known that the structural vibration produces a high degree of span-wise correlation, giving rise to nearly 2-D flow for an elastically mounted cylinder subjected to flow, so that 2-D numerical simulations are of more value under this condition than for fixed body problems. In the earlier studies, a longer correlation length was considered to be associated with larger response (Pantazopoulos, 1994). In fact, a high correlation does not necessarily correspond to large amplitude response. Hover et al. (2004) "surprisingly" found in physical experiments that the span-wise correlation undergoes a sharp reduction near the region with maximum amplitude where the phase angle ϕ is undergoing transition. These findings were confirmed by Lucor et al. (2005) with 3-D numerical simulations. In addition, Hover et al. (2004) concluded that high mass and damping reinforce correlation during such transition, whereas low values admit a correlation loss; their study may help our understanding on the response characteristics in the upper branch and the transition between the upper and lower branches. One may note that the region with poor correlation overlaps well with the upper branch. The upper boundary of this region might correspond to the beginning of the lower branch with the recovery of higher correlation.

The time-dependent series of the fluid forces and the structural response, associated with vortex shedding, should be treated as random processes. The span-wise correlation is an indicator to the degree of three-dimensionality of the wake and might relate to the statistical characteristics of the fluid forces and the cylinder displacement. A high level of correlation might restrain the randomness of the vortex shedding and bring on a periodic response, whereas poor correlation might result in the variation in response amplitudes. Experimental results show that the response in the upper branch is less periodic and is subjected to more random disturbance than that in the lower branch. Such distinctions are more remarkable with smaller m^* and ζ (Khalak and Williamson, 1999; Govardhan and Williamson, 2000).

It is difficult to formulate the random characteristics of the fluid forces and the cylinder response. Therefore, the following linearized representation for the self-excited motion of a cylinder and the corresponding unsteady force still prevail in the relevant literature:

$$y = A\sin(\omega_{ex}t), \tag{1}$$

$$C_y = C_L \sin(\omega_{ex} t + \phi), \tag{2}$$

$$C_{Lv} = C_L \sin \phi \text{ and } C_{La} = -C_L \cos \phi, \tag{3}$$

where y is the transverse displacement and ω_{ex} is the oscillation frequency; C_y, C_L, C_{La} and C_{Lv} represent the unsteady lift force coefficient, its amplitude and components in phase with acceleration and velocity, respectively. The response amplitude and frequency can be derived according to Parkinson (1974) as follows:

$$\frac{A}{D} = \frac{1}{4} \frac{C_{Lv}}{\pi^3 m^* \zeta} \frac{f_n}{f_{ex}} \left(\frac{U}{f_n D} \right)^2, \tag{4}$$

$$\frac{f_{ex}}{f_n} = \frac{1}{\sqrt{1 + C_a/m^*}}, \tag{5}$$

where $f_{ex} = \omega_{ex}/2\pi$, and C_a is the added mass coefficient relating to C_{La}; see Gopalkrishnan (1993). Slightly different forms of the above two equations were proposed by Khalak and Williamson (1996, 1999) and Govardhan and Williamson (2000). Whatever forms are employed, it should be noted that these equations originate from the linearization of the cylinder oscillation with energy balance between the structure and the surrounding fluid. Therefore, they may be more appropriate to represent the averaged amplitude ratio and corresponding mean frequency ratio.

Previously, VIV was largely investigated by experiments. However, with the recent improvements in computing and storage capabilities, more research activities on VIV have turned to CFD techniques. Currently, there have been primarily three different computational approaches in the open literature toward describing the flow field and forces for this problem, namely Reynolds-averaged Navier–Stokes (RANS), Large Eddy Simulation (LES) and Direct Numerical Simulation (DNS). Although DNS and LES provide a much deeper insight in the wake-boundary-layer interaction mechanism compared to RANS simulation, as was noted by Sarpkaya (2004), RANS codes are more robust, less time-consuming and have been applied as practical design analysis tools with reliable solutions. Guilmineau and Queutey (2004) used a RANS code to simulate a case experimentally investigated by Khalak and Williamson (1996). They predicted a 2P mode in the lower branch and a high amplitude of response. However, they did not give explanations on several details, which are not consistent with the experimental results, such as: the absence of the upper branch; one frequency response everywhere; and much lower frequency in the lock-in region.

It is worth noting that Reynolds-averaging procedure erases the random disturbances in RANS calculations, so that the fluid forces and the body response tend to be quite repeatable in the lock-in region. One may argue that such RANS simulation results do not agree with those from experiments. However, careful comparison between the numerical results and the experimental data may help us assess the effects of random disturbance in the time series of forces and displacement in experiments and those in DNS/LES. Furthermore, we can avoid the impatient wait for the longtime random process evolutions in DNS/LES. The linearized formulations, i.e., Eqs. (1)–(5), are more easily applied in the analysis of the results obtained by RANS simulations (as can be found in the present paper).

In this paper, numerical simulations are presented for the transverse response of an elastically mounted cylinder subjected to VIV in a uniform flow with a RANS solver. The physical parameters are the same as those in Khalak and Williamson (1996, 1999): $m^* = 2.4$ and $m^*\xi = 0.013$; except for the 2-D simplification. We changed U^* from 3.0 to 14.9 with increasing velocity. The corresponding Reynolds number is from 2500 to 13 000. We concentrate on the response and fluid forces acting on the cylinder. We also investigate the existence and transition of the 2P vortex-shedding mode throughout the lock-in region. The results are compared with experiments performed by Khalak and Williamson (1996, 1999) and numerical results from Guilmineau and Queutey (2004).

2. Numerical method

The fluid flow computation is in the framework of the Finite Volume Method (FVM). The RANS equations can be written as

$$\frac{\partial u_i}{\partial x_i} = 0, \tag{6}$$

$$\frac{\partial}{\partial t}(\rho u_i) + \frac{\partial}{\partial x_j}(\rho u_i u_j) = -\frac{\partial p}{\partial x_i} + \frac{\partial}{\partial x_j}\left(2\mu S_{ij} - \rho \overline{u_j' u_i'}\right), \tag{7}$$

where u, p represent the time-average value of velocity and pressure; μ is the molecular viscosity, and S_{ij} is the mean stress tensor. The small-scale fluctuations of velocity relating to the turbulence are reduced as $\overline{u_j' u_i'}$, which is referred to as the Reynolds stresses. The shear stress transport (SST) $k-\omega$ turbulence model is used in the present work. It models the Reynolds stresses with two transport equations for the turbulent kinetic energy k and the specific dissipation rate ω. The SST $k-\omega$ model shows good performance in predicting the adverse pressure gradient flows. One can refer to Menter (1994) for a detailed description of this model. The unsteady segregate solution is adopted in the calculations. The SIMPEC algorithm is used to solve the pressure-velocity coupled equations. The implicit first-order scheme is used for the unsteady terms. The third-order upwind difference scheme QUICK is applied to the convection terms in the momentum equations and a second-order scheme for the k and ω transport equations. For the diffusion terms, the central difference scheme is applied. These numerical algorithms are quite standard now. In the present work, the same turbulence model is taken as that by Guilmineau and Queutey (2004) with some differences in other specific techniques.

The hybrid unstructured meshes are used in the present calculations. A fine grid is created near the cylinder and gradually coarser in the wake and in the far field. The whole computational domain is discretized as shown in Fig. 1. The left part is semicircular with the dimension about $10D$ in the r direction, whereas the right part is square with borders $20D$ in length. The flow runs from the left to the right. The inflow boundary (the outer boundary of the semicircular and the upper/lower borders of the square) is specified with the inflow velocity. On the right exit boundary, the hydrostatic pressure is given. The no-slip condition is employed on the cylinder surface. The first points of the mesh in the fluid are located near the wall where y^+ is about unity. Grid independence tests were performed giving the result with 120 nodes around the cylinder and 13 482 mesh points in all. The normalized time step τ ($=tU/D$) was set to be 0.0025 in the calculations.

The fluid force obtained by solving the RANS equations is coupled with the motion of the cylinder. According to Guilmineau and Queutey (2004), the following equation may represent the transverse response of an elastically mounted cylinder subjected to VIV:

$$\frac{\mathrm{d}^2 Y}{\mathrm{d}\tau^2} + \frac{4\pi\zeta}{U_r}\frac{\mathrm{d}Y}{\mathrm{d}\tau} + \frac{4\pi^2}{U_r^2} Y = \frac{2C_y}{\pi m^*}, \tag{8}$$

in which $Y = y/D$ is the normalized displacement. The response of the cylinder is obtained by taking the fluid force as the input for the right-hand side of the equation. The forcing term (on the right-hand side) is assumed to be a constant within a sufficient small time step. Thus, Eq. (8) can be integrated in time using a fourth-order Runge–Kutta algorithm. The fluid dynamic force and the body motion are solved in a coupled way in the moving reference frame with the origin located at the center of the cylinder. As a result, an additional time-dependent source term should be added to the momentum Eq. (7), and the inflow boundary condition should be adjusted at every time step according to the transverse velocity of the cylinder.

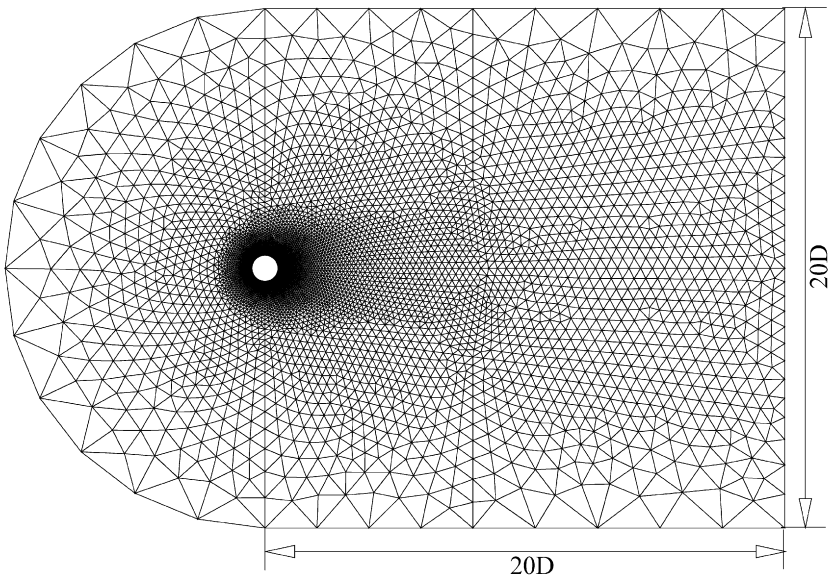

Fig. 1. Computational grid.

3. Results and discussion

3.1. Response and force

The normalized amplitude and frequency ($f^* = f_{ex}/f_{wtr}$) response as a function of U^* is given in Fig. 2 together with the experimental results. These data were derived from the displacement time series, shown in Figs. 3(a)–(e) for some selected cases with different U^*, together with time traces of the lift and drag forces.

The beating behavior of the displacement and lift force can be seen in Fig. 3(a) and the left part of Fig. 3(b). The lift force and the vibration, with varying amplitude in the range denoted by vertical bar in Fig. 2(a), are dominated by two major frequencies, which are obtained by FFT analysis: one corresponds to f_{wtr} and the other corresponds to f_{st} (Strouhal frequency of the fixed cylinder). The phase angle ϕ exhibits "slipping" in Fig. 3(a), whereas maintains about 0° in the left part of Fig. 3(b). These results are consistent with the description of the initial region by Khalak and Williamson (1999). They characterized these two beating phenomena as "quasi-periodic" and "periodic" (approximately) in two different sub-regions. However, Guilmineau and Queutey (2004) did not provide similar results in the initial branch.

It should be noted that the increment step in U^* was originally set to be 0.2. We found that the response shifted to another state from initial branch when $U^* = 4.2$. Then we gradually reduced the step to 0.025, and the response shift was postponed to $U^* = 4.40$, as shown in Fig. 3(b). At such transition, the amplitude reaches a maximum $A^* = 0.70$ [with a jump and then fall off, shown in Fig. 2(a)]. With several periods of self-regulation, the system arrives at a steady state, in which the response amplitude ($A^* = 0.54$) and forces are almost periodic. During the transition, the amplitude of lift force decreases, whereas the amplitude and the mean value of the drag force jump up. However, the phase angle is preserved at about 0° after the transition [see the right part of Fig. 3(b)]. The maximum value of A^* is often of interest to many researchers. The magnitude $A^* = 0.70$ is smaller than that from Guilmineau and Queutey (2004) ($A^* = 0.98$). However, Khalak and Williamson (1999) did not find the maximum A^* at this point but at a higher U^*. Moreover, in contrast to Guilmineau and Queutey (2004), it is not a stable state when the maximum A^* is reached in our study.

Over the region $U^* = 4.4$–11.0, we observed that the cylinder vibrated at a certain frequency and a magnitude of amplitude for each U^*, indicating that the vortex shedding frequency was fully locked on to f_{ex} [see Figs. 3(b)–(d)]. It is

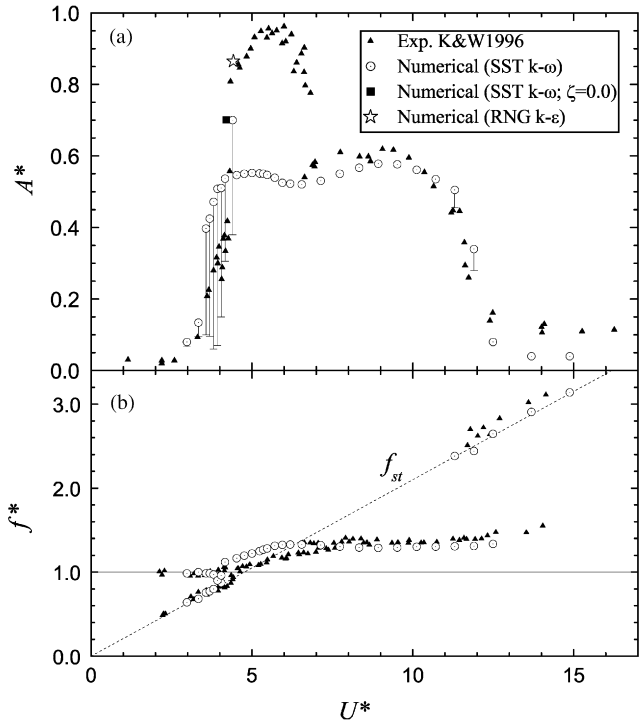

Fig. 2. Response amplitude and frequency versus reduced velocity U^*, for $m^* = 2.4$ and increasing velocity (vertical bars representing the beating behavior with varying amplitude).

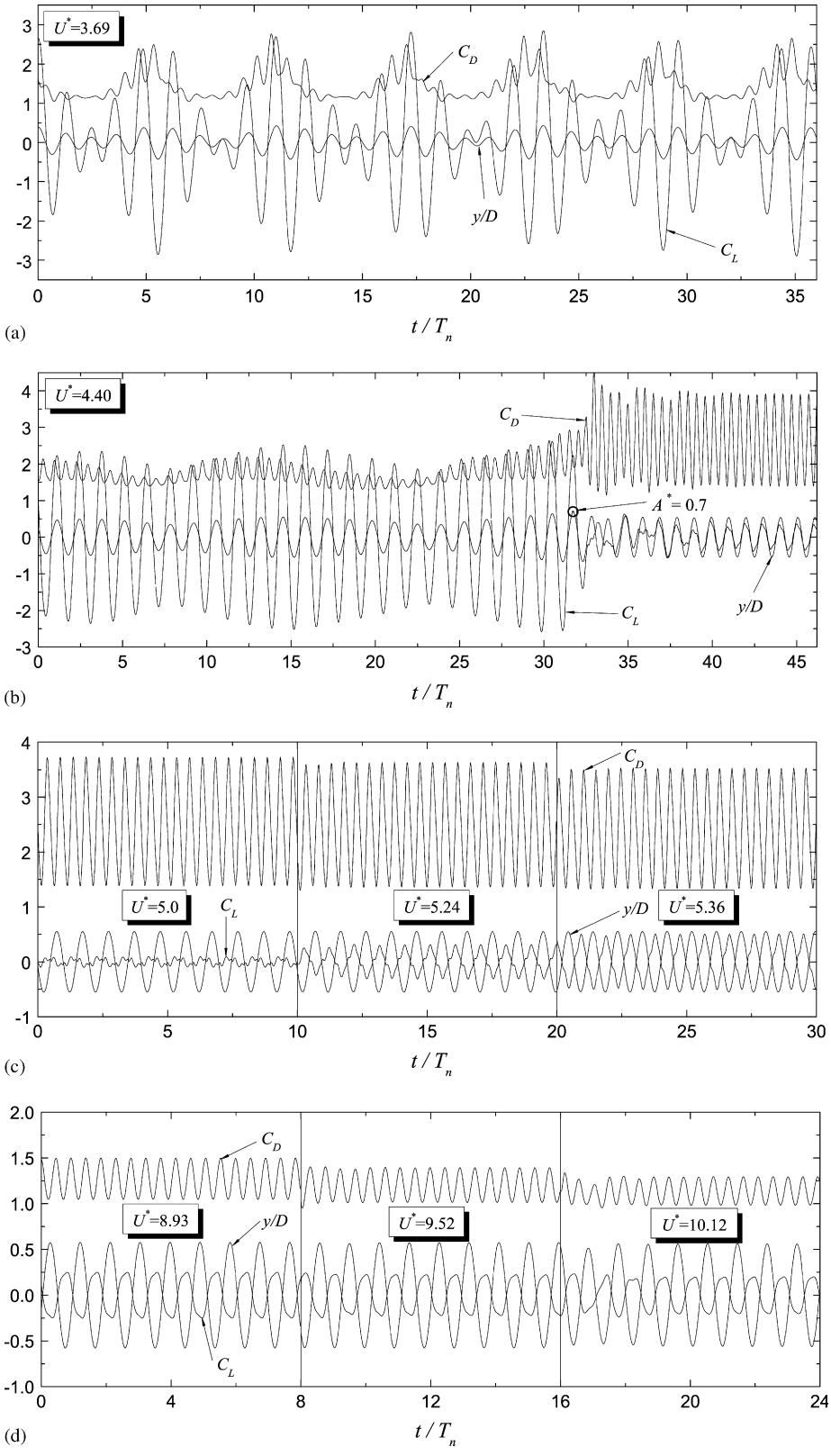

Fig. 3. Force and displacement time histories at different reduced velocity. Horizontal axes represent normalized time by $T_n = 1/f_n$.

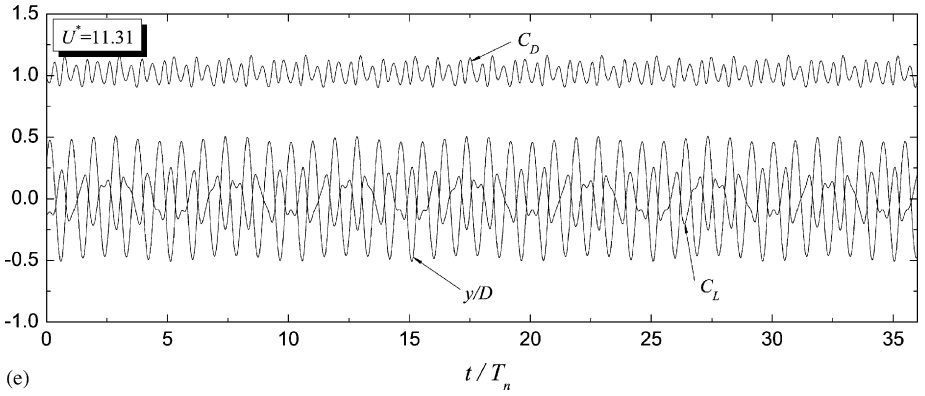

Fig. 3. (*Continued*)

assumed that this region corresponds to the lock-in region, i.e., the combination of the upper and lower branches in experiments. At each U^* in this region, the displacement is nearly sinusoidal, whereas the transverse force is relatively irregular, especially in the left side where phase angle is in transition. Similar to Guilmineau and Queutey (2004), the upper branch is also absent in our results [see Fig. 2(a)]. In the lock-in region, the amplitudes change in the range of 0.52–0.58, with the higher U^* part overlapping well the lower branch in Khalak and Williamson (1996, 1999). On the other hand, the frequency ratio f^* goes smoothly from 1.05 to about 1.35. The response frequency in the lower branch agrees well with experimental results (Khalak and Williamson, 1996). In addition, the amplitude and mean value of the drag force decrease with increasing velocity. Consistently with the measurements in Khalak and Williamson (1996, 1999), the mean drag force goes down from about 2.8 to 1.1 in the lock-in region.

When $U^* = 11.31$, the oscillation of the cylinder and fluid force appear not periodic again, indicating the end of lock-in state [see Fig. 3(e)]. We can find in the lift force spectra two peaks again, one at f_{ex}, the other at f_{st}. With further increase of the inflow velocity, the amplitude falls to a small magnitude and the system is locked out.

In fact, only about 1/5 computation time was spent in the lock-in region where the steady state can be obtained within about 10 periods of oscillation when U^* is changed. The amplitude of the cylinder motion and the fluid forces are quite repeatable from cycle to cycle when the final solution is reached for each U^*. On account of this, the equivalent fluid force components and phase angle can be deduced, as shown in Figs. 4(a)–(d), with relatively exact values of A^* and f_{ex} through Eqs. (1)–(5):

$$C_{Lv} = 4\pi^3 m^* \zeta U_r^{-2} A^* \frac{f_{ex}}{f_n}, \tag{9}$$

$$C_{La} = 2\pi^3 \left[\left(\frac{f_{ex}}{f_n} \right)^2 - 1 \right] m^* U_r^{-2} A^*, \tag{10}$$

$$C_a = -\frac{C_{La}}{2\pi^3 \left(f_{ex} D/U \right)^2 A^*}, \tag{11}$$

$$\phi = \arctan\left(-C_{Lv}/C_{La} \right). \tag{12}$$

As can be seen in Fig. 4(a), C_{Lv} is rather small throughout the lock-in region, indicating that the power absorption from the surrounding fluid is very low for this low mass-damping ($m^*\xi = 0.013$) case. However, C_{La} is changing within the range -1.0 to 1.0 [see Fig. 4(b)], corresponding to the transition of C_a from about 0.3 to -0.5 [see Fig. 4(c)]. According to Eq. (5), the change of C_a and the low m^* are responsible for the departure of the frequency response from unity in the lower branch, which is more accurately predicted in the present study than in Guilmineau and Queutey (2004) [see Fig. 3(b)]. Fig. 4(d) shows that the fluid force and the cylinder displacement are gradually out of phase in the left side of the lock-in region. The transition of ϕ can also be observed in Figs. 3(b)–(c), although the lift force is quite irregular in shape in this zone. In most of the lock-in region (higher value side), ϕ is maintained at slightly below 180°, much smoother than the result of Guilmineau and Queutey (2004).

Now, we concentrate on the response amplitude in the left part of the lock-in region where the upper branch in the experiment is absent in the present numerical results. The reason why the upper and lower branches emerge as one

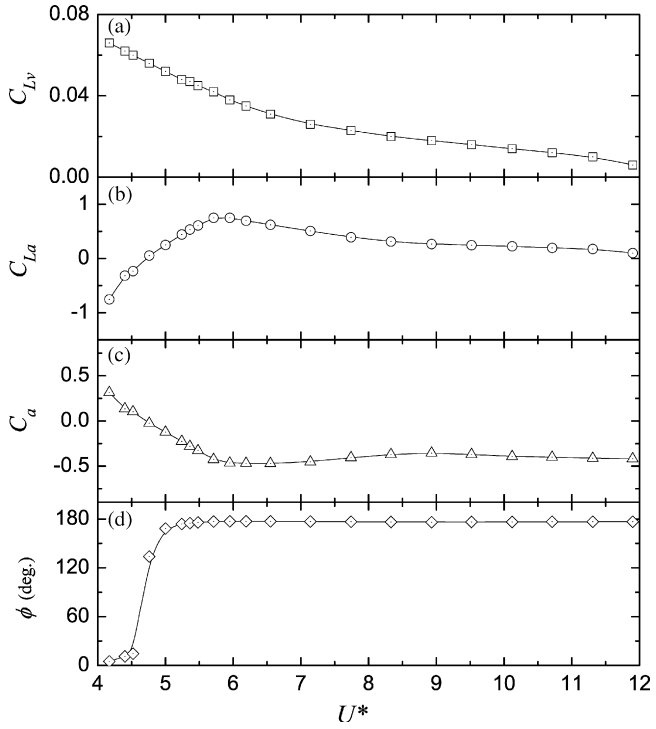

Fig. 4. Coefficients of the equivalent fluid force components, added mass and phase angle in the lock-in region.

branch in 2-D RANS simulations will be investigated. To this end, both the experimental facts and the built-in features of the 2-D RANS solver should be re-examined. The following four issues, associated with each other, determine the appearance of the upper branch in experiments.

Firstly, the upper branch corresponds to the region where the span-wise correlation of the wake and forces are apparently lower than outside this zone, according to the investigations carried out by Hover et al. (2004) and Lucor et al. (2005). The loss of span-wise correlation relates to the increase of three-dimensionality of the wake and more remarkable random disturbance in the time series of the fluid forces and the cylinder response. The random behavior in the response is largely restrained in the upper side of this region, namely the lower branch in the experiments. Khalak and Williamson (1996, 1999) found that "the response is very periodic and looks like a pure single frequency" on the lower branch. A part of the reason may be that the wake is correlated well and randomness is depressed. Lucor et al. (2005) indicated a Reynolds number dependence of the amplitude and the range of the upper branch. It is indicated that the Reynolds number relates to the degree of the instability in the vortex-shedding process so that it may be the most important parameter involving the random characteristics of vortex-shedding-related problems.

Secondly, the lower m^* and ξ add to further loss of span-wise correlation in this region, as suggested by Hover et al. (2004). One can infer that the lighter body may react more noticeably to the change of the fluid force. The reaction of the structure may in turn feed back to the flow and increase the irregular behavior of the vortex-shedding process. As a result, a cylinder with low m^* and ξ can never arrive at the short-term power balance state on the upper branch in the experiments.

Thirdly, we can further deduce that the short-term response of the cylinder in VIV may not accord with a fixed U^* due to the random disturbance. In other words, the same short-term response may occur over a range of U^*, whereas only the total response characteristics may correspond to a certain U^* value. In light of this, we would rather describe the response at the "upper branch" as "intermittent switching" between the initial and lower branches than between the upper and lower branches. The switching corresponds to the amplitude reaching an instantaneous maximum value (shown in the amplitude response figure as a jump from both sides), which may occur over a region of U^*. In the left side of the lock-in region, the cylinder is more likely to undergo such a switching, whereas the switching rarely happens in the right side of the "upper branch". The amplitude ratio A^* is defined by Khalak and Williamson (1996, 1999) as the maximum value in the time trace [different from Hover et al. (2004) and Lucor et al. (2005) who used 1/10 of the highest averaged value]. If we redefine A^* as the averaged (or root-mean-square) amplitude, almost all of the existing figures of

amplitude response should be redrawn. An example is provided by Khalak and Williamson (1999), as shown in Fig. 16 therein, where the upper and lower branches are combined. In fact, such "intermittent switching" also happens in high $m^*\xi$ case, as shown in Fig. 9 in Govardhan and Williamson (2000). However, in that case, the switching takes a longer time interval, and the response is less affected by the random disturbance. One can compare the time traces of response at the upper branch for different m^* presented by Govardhan and Williamson (2000) in Fig. 22 therein. They also imply that low m^* and ξ add to the randomness.

Fourthly, one should note that "the range of synchronization is controlled primarily by m^*", as Khalak and Williamson (1999) found. It can be inferred that the range of the "upper branch" is also controlled by m^*, so that lower m^* is associated with a broader region of the upper branch [see, e.g., Fig. 6 in Khalak and Williamson (1999)]. Moreover, the upper branch would be shrunk to nearly "one point" at the end of the initial branch for high $m^*\xi$ cases, as the results in Feng (1968).

The reason for the absence of the upper branch is obvious if we compare the present numerical simulation results with the experimental facts. Here, the calculation is constrained in the 2-D domain, indicating that the fluid force is always in a perfect spanwise correlation. Without reference to the physical parameters m^*, ξ and U^*, the RANS method has erased the random disturbances, giving rise to a repeatable fluid force and response in the lock-in region. With given m^* and ξ, the response and force would be almost a function of U^*, apart from the hysteretic region at the end of the initial branch. We can see that the amplitude response obtained by RANS simulations is more similar to the result provided by Feng (1968) with high $m^*\xi$. It is suggested that the appearance of the upper branch would rather be controlled by the degree of irregular behavior in the vortex-shedding process, which is coupled with the body response. It should be noted that the Reynolds-averaging has saved a large amount of CPU time and data postprocessing time as well, so that we can perform all the simulations in a personal computer (CPU AMD 3000+ and 1G DDR RAM).

The quest for the maximum attainable amplitude is still on-going for a cylinder undergoing VIV, as noted by Williamson and Govardhan (2004). Khalak and Williamson (1999) speculated that the largest amplitude would be obtained by the CFD method, for ξ can be set to zero in numerical simulations. However, the largest amplitude rarely exceeds 1.0 in CFD simulations in spite of $\xi = 0$; see, e.g., Lucor et al. (2005) for a case with $m^* = 2.0$. In the present study, we obtain $A^*_{\max} = 0.70$ as an instantaneous value at the end of the initial branch (with a jump in amplitude), apparently lower than experimental results $A^*_{\max} = 0.96$. This (together with the absence of the upper branch) frustrated us at the beginning of the present numerical work. When we set ξ to zero at the same U^*, the results remained unchanged. We then resorted to another turbulence model, RNG $k-\varepsilon$ model. A higher value $A^*_{\max} = 0.85$ was obtained with pure sinusoidal oscillation [see Fig. 2(a)]. These attempts indicate that the $A^*_{\max}$ is only dependent on the numerical techniques in CFD simulations. For the case with lower enough $m^*\zeta$ (0.013), $A^*_{\max}$ would not increase further even if ζ is set to be zero. It can be inferred that, in the experiments, $A^*_{\max}$ increases with decreasing $m^*\zeta$, owing to the increased random behavior of the response. In numerical simulations, the $A^*_{\max}$ is lower because the random disturbance may be reduced or erased. Shorter computational time in LES and DNS than that in experiments could be another reason. In contrast with the present RANS simulations without the random disturbance, the displacement of a cylinder undergoing VIV in experiments is a random process, so that the longer observation time may result in witnessing a larger attainable amplitude. According to the above discussion on the maximum amplitude and the absence of the upper branch, it may be suggested that if $A^*_{\max}$ is redefined as the average amplitude; the maximum value (when $\zeta = 0$) might be located in the region 0.7–0.9 at the end of the initial branch. This value may be more comparable to the maximum A/D with positive C_{Lv} in the forced-oscillation cases [see, e.g., Gopalkrishnan (1993) and Hover et al. (1998)]. It is unreasonable to compare these two values directly. Apparently, the former value is certainly relatively larger than the later one. One should note that the maximum A/D with positive C_{Lv} in the forced-oscillation is less affected by the random disturbance and corresponds to the state with power balance (within many periods of oscillation) between the fluid and the cylinder. The above discrepancy between the results from the forced and free oscillation tests should be considered in developing prediction tools for VIV of marine risers; see relevant report from 14th ISSC (2000).

3.2. Modes of vortex formation

The vortex formation in the wake of an oscillating cylinder is associated with the amplitude ratio A^* and the reduced frequency f_r ($= f_{ex}D/U$), as suggested by Williamson and Roshko (1988). Although it remains as an unsettled problem for the relationship between the vortex-shedding modes in forced oscillations and those in self-vibration (Carberry et al., 2004), the map of the wake modes from Williamson and Roshko (1988) is widely applied in both cases. As noted by Al Jamal and Dalton (2005), the irregular forces and displacement indicate that the time required for repeatable vortex structures probably is not met, and "expected" wake modes (2S/2P) are not generated. According to the discussion in the above paragraphs, the response would be intermittently switching between the initial and lower branches on the

"upper branch" in experiments and in LES/DNS simulations. Therefore, the resulting vortex shedding formation in the wake would be mixed with the 2S mode and the 2P mode. The loss of the spanwise correlation of the wake is also evidence of the competition between different vortex shedding modes. Lower m^* or ζ would further complicate the situation. Govardhan and Williamson (2000) observed a repeatable 2P mode in the upper branch with $m^* = 8.63$. If the m^* had been reduced to about 2.0, their study might be more difficult with more remarkable irregular behavior in the fluid force, displacement, and, of course, in the vortex shedding pattern. However, the irregular phenomenon is quite restrained and the response would not switch to the initial branch (with 2S mode) for the lower branch with higher U^* value. In these cases, the observation of the 2P mode is easier in both experiments and LES/DNS simulations; see Blackburn et al. (2001) and Lucor et al. (2005). In the present study with a 2-D RANS code, the irregular phenomenon in the vortex shedding process is eliminated, giving rise to almost periodic force and response throughout the lock-in region. Once shifted into the lock-in state from the initial branch, the response would never switch back in RANS simulations! Thus, the upper branch is absent and we can investigate the vortex formation in the wake for each U^* without the random disturbance. Khalak and Williamson (1999) did not provide the detailed information on the vortex patterns. Therefore, we compare our results to those given by Govardhan and Williamson (2000).

The predicted shift from the initial branch to the synchronization state [see Fig. 3(b)] indicates a shift of the vortex formation. Likewise, the transition through the lock-in region [see Figs. 3(c)–(d)] is associated with the gradual change of the vortex shedding mode. These judgments can be made by examining the vortex patterns for different U^* shown in Figs. 5–8.

Three groups of the vorticity plots are shown in Figs. 5–7, corresponding respectively to the wake structures in the initial branch, the left side of lock-in region with lower U^*, and the right side of lock-in region with higher U^*. They are compared with the DPIV results obtained by Govardhan and Williamson (2000) for the initial, upper and lower branches in experiments. The classical 2S vortex formation mode is shown in Fig. 5 for $U^* = 3.93$. We found that even

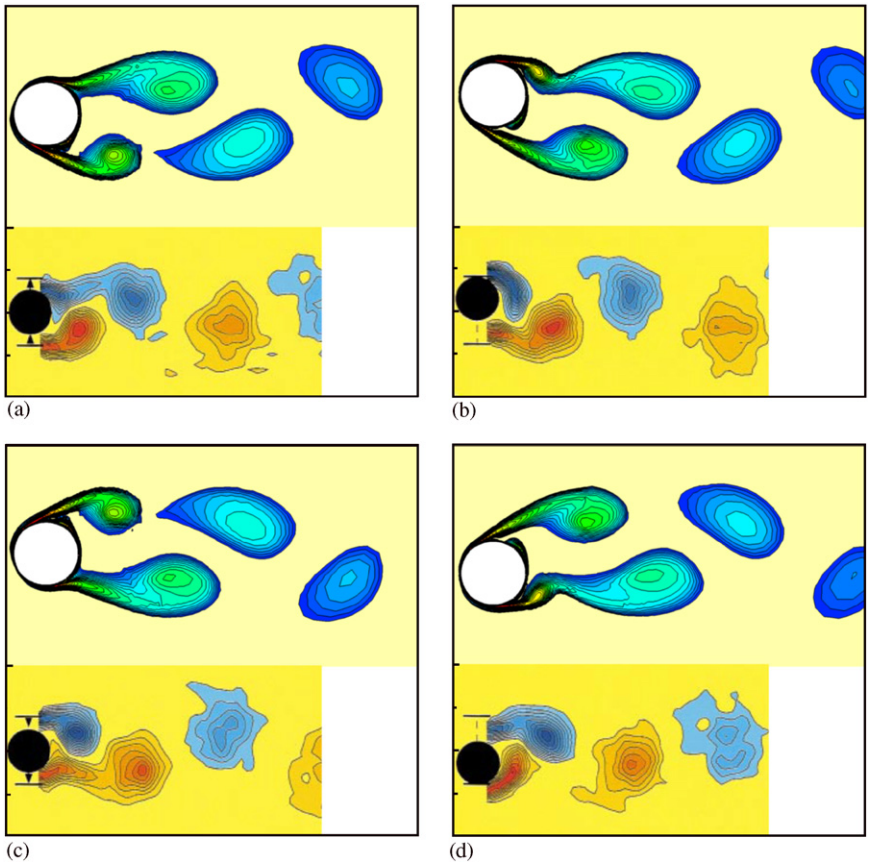

Fig. 5. The vorticity contours showing the 2S mode (corresponding to the initial branch) compared with the DPIV results by Govardhan and Williamson (2000). ($A^*_{\text{average}} = 0.30$, $U^* = 3.93$, $\text{Re} \approx 3400$).

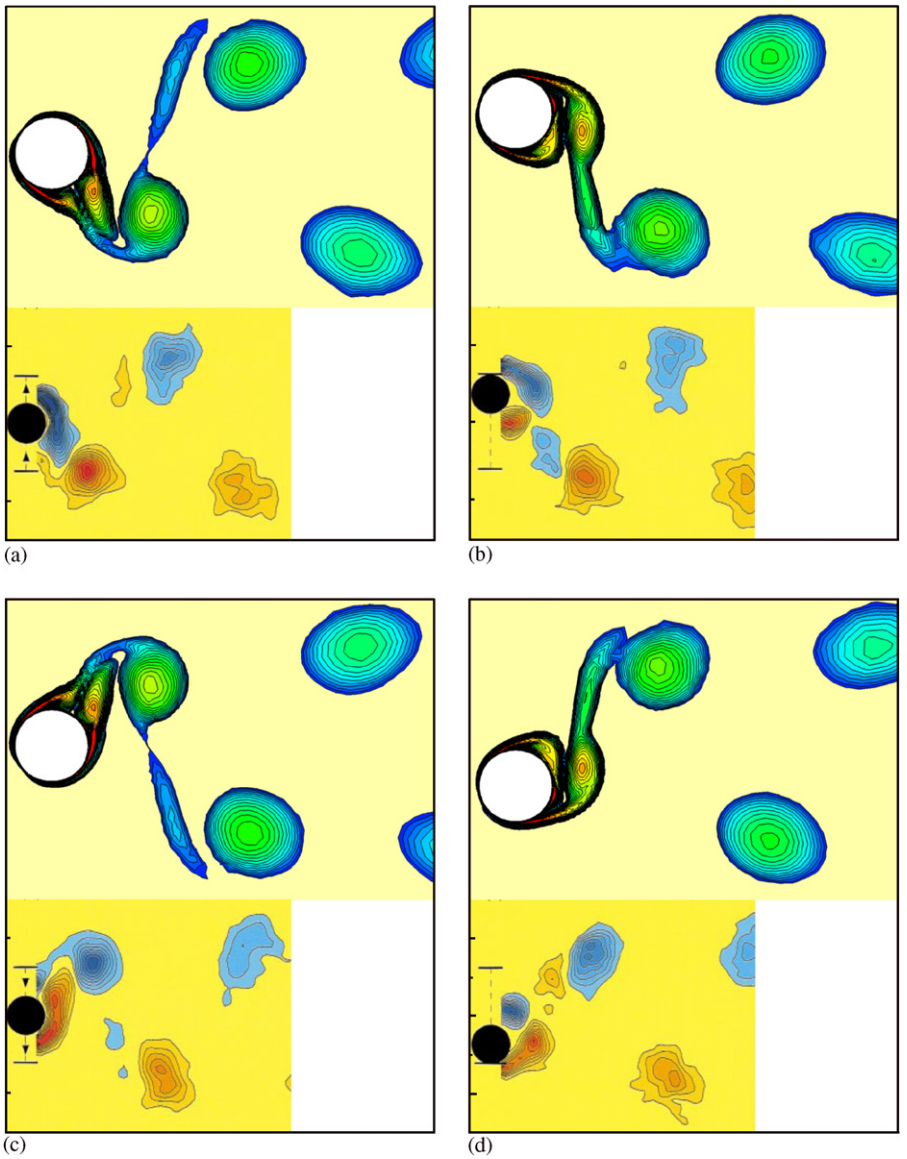

Fig. 6. The vorticity contours showing the 2P mode (corresponding to the upper branch) compared with the DPIV results by Govardhan and Williamson (2000). ($A^* = 0.544$, $U^* = 4.40$, $\mathrm{Re} \approx 3800$).

at the shifting process when the amplitude climbed up to $A^* = 0.7$, the vortex shedding still remained as the 2S mode. However, after some period of regulation in the fluid forces and the response [see Fig. 3(b)], the system arrived at the synchronization state, and the 2S mode changed into the 2P mode, shown in Fig. 6. Although, the amplitude is lower than that in experiments, the vortex formation is in good agreement with the description by Govardhan and Williamson (2000): "a second vortex pair is rapidly weakened by the relatively stronger first vortex." Moreover, comparison between Figs. 5 and 6 indicates that there is a clear change in the "timing of vortex shedding" between the two groups of vorticity plots. Govardhan and Williamson (2000) stressed that the phase angle remains near 0° for the "upper branch". This is also consistent with present numerical results [see the left part of Fig. 3(b) as well as Fig. 4(d)]. Fig. 7 shows another pattern of the 2P mode, now that the two vortex pairs are comparable in strength. The "timing of vortex shedding" is the same for Figs. 6 and 7, whereas the corresponding phase angle has changed by about $+180^\circ$ [see Fig. 4(d)].

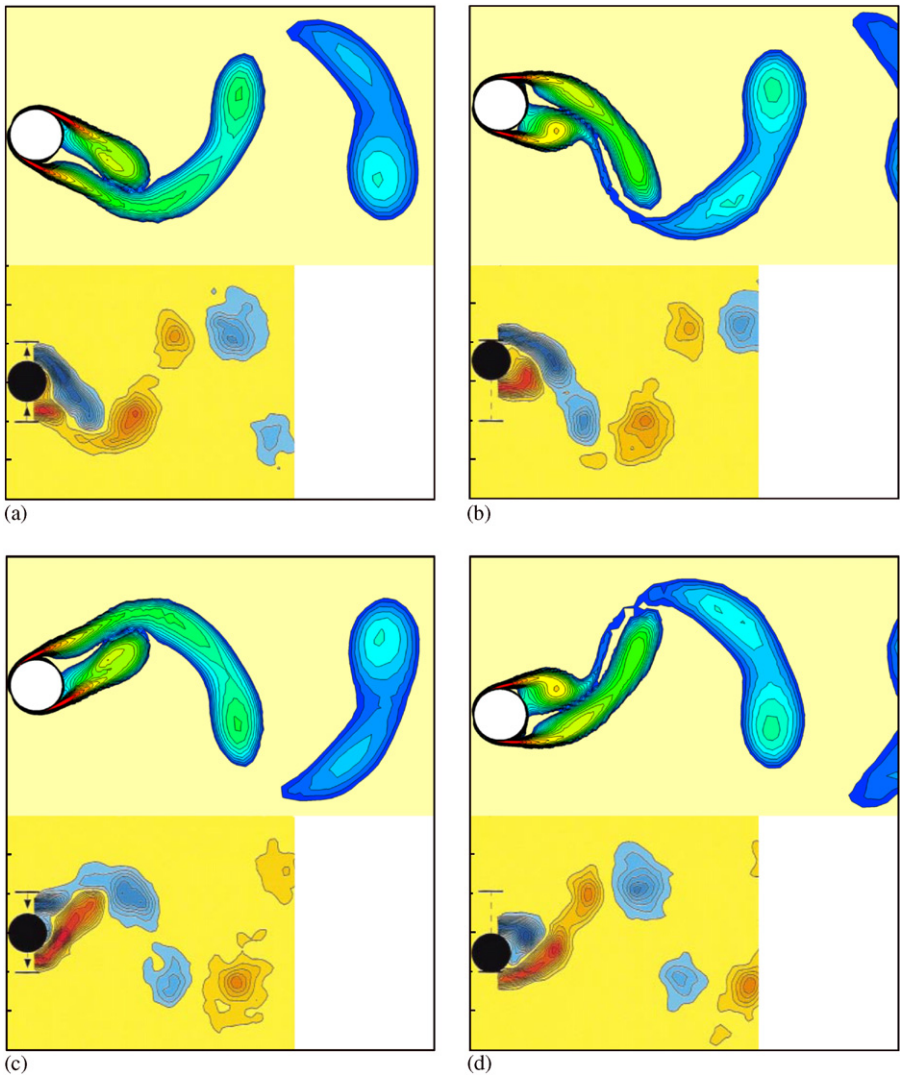

Fig. 7. The vorticity contours showing the 2P mode (corresponding to the lower branch) compared with the DPIV results by Govardhan and Williamson (2000). ($A^* = 0.566$, $U^* = 8.33$, $\mathrm{Re} \approx 7200$).

The transition of the vortex formation in the lock-in region is presented in Fig. 8, indicating that the wake pattern sets out as the shape shown in Fig. 6, then changes gradually into the shape described in Fig. 7 through the synchronization zone. As U^* is increased, the vortices stretch along the centerline of the wake and the second vortex pair grows in strength. According to the map of wake modes in Williamson and Roshko (1988), the vortex mode is mainly determined by A^* and f_r. This suggests that in the present study the vortex mode is mostly dependent on f_r in the free-oscillation case, since A^* maintains at about 0.55 in the lock-in region. On account of this, we provide f_r for the each plot in Fig. 8 for reference. It shows that f_r decreases as U^* increases.

Apart from A^* and f_r, the vortex mode also relates to its past and prevailing state. That is to say, a certain vortex mode tends to maintain its history state when the external condition has been changed. This character may be responsible for the hysteresis in free vibration experiments and the indefinite location of the critical curve in the wake modes map from forced-oscillation tests. However, the random characteristic of the vortex-shedding process complicates the entire problem. It results in the irregular changing of the wake structure, as well as the random disturbance in time series of the fluid force and the body response. Obviously, owing to the Reynolds-averaging procedure, the vortex shedding is statistically stable in the present RANS simulations, so that VIV problems can be investigated without random disturbances.

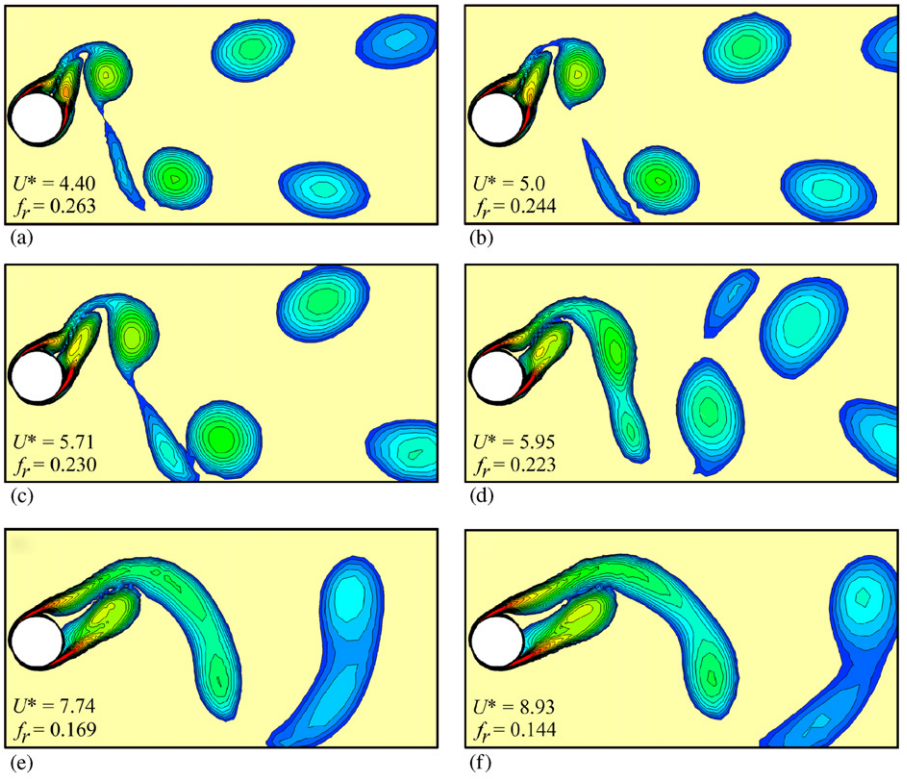

Fig. 8. The vorticity contours in the wake at different reduced velocity in the lock-in region (the cylinder at the center of its transverse oscillation moving downwards; $\mathrm{Re} \approx 3800$–7700).

4. Summary and conclusions

In this paper, the transverse vortex-induced vibration (VIV) of an elastically mounted cylinder at low mass and damping is extensively investigated with a RANS code equipped with the SST $k-\omega$ model. The fluid forces, cylinder response and the vortex mode in the wake are in good agreement with the experimental results.

The random disturbance with the vortex shedding process handicaps our understanding on the response characteristics of a cylinder subjected to VIV. The loss of the span-wise correlation and the low value of $m^*\xi$ add to the random disturbance, especially for the left side of the synchronized region overlapping with the upper branch, where phase angle is shifting. We suggest that the response in the upper branch may be associated with "intermittent switching" between the initial and lower branches, so that the 2P/2S-mixed vortex shedding mode is observed in experiments and in LES/DNS simulations. The appearance of the upper branch relates to the irregular behavior of the response, the value of m^* and ξ, as well as the approach used in recording the amplitude response.

The random disturbance is erased by the Reynolds-averaging procedure, so that RANS simulation results are statistically stable. The discrepancies between the numerical results and the experimental data originate from the irregular behavior of the response, forces, and vortex formation in the wake for a cylinder in VIV. In the present work, the response is quite periodic when the final solution has been reached at each U^* in the lock-in region, and the intermittent switch does not occur between the initial branch and the synchronization region. The disparity in the random behavior between experiments and the results obtained by RANS codes may explain the absence of the upper branch in this study.

The response amplitude reaches its maximum at the upper end of the initial branch, which is next to the beginning of the lock-in region. Further decrease of ξ does not increase the maximum amplitude for low $m^*\xi$ cases in the RANS calculations. For cylinder with low $m^*\xi$, the intensified irregular behavior in the response may be responsible for the increase of the maximum amplitude in experiments with further decrease in m^* or ξ. The maximum amplitude in free oscillation experiments should not be compared with the maximum A/D with positive C_{Lv} in forced-oscillation tests, before the random behavior of free oscillation is reasonably considered.

The different 2P modes reproduced in this study are consistent with the experimental results in the upper and lower branches. The vortex mode changes gradually across the lock-in region, associated with the change of the frequency ratio.

It is suggested that the random characteristics of the vortex-shedding process and the body response should be further investigated and formulated. The Reynolds number may be the most important influencing parameter. Lower m^* and ξ add to the random behavior of the body response. The loss of the spanwise correlation may be associated with the increase of the irregular behavior of the fluid forces and the vortex shedding mode. Further numerical investigations with 3-D RANS codes are needed, especially for the correlation loss region.

The CFD method has become an indispensable complement to experiments in ocean engineering. The present work shows that the RANS code can be used in the prediction of VIVs of a 2-D circular cylinder. Coupled with the strip method, or taken as the input for other VIV analysis tools with numerical free/forced oscillation tests, such methods can be used to predict the VIV of slender marine risers.

Acknowledgments

We are grateful to Professor Charles H.K. Williamson for his kind help and discussions. We have also benefited from the interactions with Professor Raghuraman N. Govardhan and Mr Emmanuel Guilmineau. This project has been supported by the National Natural Science Foundation of China (No. 50323004) and a Grant from the Science & Technology Commission of Shanghai Municipality (No. 05DJ14001).

References

Al Jamal, H., Dalton, C., 2005. The contrast in phase angles between forced and self-excited oscillations of a circular cylinder. Journal of Fluids and Structures 20, 467–482.

Blackburn, H., Govardhan, R., Williamson, C.H.K., 2001. A complementary numerical and physical investigation of vortex-induced vibration. Journal of Fluids and Structures 15, 481–488.

Carberry, J., Govardhan, R., Sheridan, J., Rockwell, D., Williamson, C.H.K., 2004. Wake states and response branches of forced and freely oscillating cylinders. European Journal of Mechanics—B/Fluids 23, 89–97.

Chaplin, J.R., Bearman, P.W., Cheng, Y., Fontaine, E., Graham, J.M.R., Herfjord, M., Isherwood, M., Lambrakos, K., Larsen, C.M., Meneghini, J.R., Moe, G., Triantafyllou, M.S., Willden, R.H.J., 2005. Blind predictions of laboratory measurements of vortex-induced vibrations of a tension riser. Journal of Fluids and Structures 21, 25–40.

Feng, C.C., 1968. The measurement of vortex induced effects in flow past stationary and oscillating circular and d-section cylinders. Master's Thesis, Department of Mechanical Engineering, University of British Columbia, Canada.

Govardhan, R., Williamson, C.H.K., 2000. Modes of vortex formation and frequency response for a freely vibrating cylinder. Journal of Fluid Mechanics 420, 85–130.

Gopalkrishnan, R., 1993. Vortex induced forces on oscillating bluff cylinders. Ph.D. Thesis, Department of Ocean Engineering, MIT, Cambridge, MA, USA.

Guilmineau, E., Queutey, P., 2004. Numerical simulation of vortex-induced vibration of a circular cylinder with low mass-damping in a turbulent flow. Journal of Fluids and Structures 19, 449–466.

Hover, F.S., Techet, A.H., Triantafyllou, M.S., 1998. Forces on oscillating uniform and tapered cylinders in crossflow. Journal of Fluid Mechanics 363, 97–114.

Hover, F.S., Davis, J.T., Triantafyllou, M.S., 2004. Three-dimensionality of mode transition in vortex-induced vibrations of a circular cylinder. European Journal of Mechanics—B/Fluids 23, 29–40.

ISSC, 2000. Structural design of pipeline, riser and subsea system, special task committee V.5 report. In: Ohtsubo, H., Sumi, Y. (Eds.), Proceedings of the 14th ISSC, vol. 2, Nagasaki, Japan.

Khalak, A., Williamson, C.H.K., 1996. Dynamics of a hydroelastic cylinder with very low mass and damping. Journal of Fluids and Structures 10, 455–472.

Khalak, A., Williamson, C.H.K., 1999. Motions, forces and mode transitions in vortex-induced vibrations at low mass-damping. Journal of Fluids and Structures 13, 813–851.

Larsen, C.M., Halse, K.H., 1997. Comparison of models for vortex induced vibrations of slender marine structures. Marine Structures 10, 413–441.

Lucor, D., Foo, J., Karniadakis, G.E., 2005. Vortex mode selection of a rigid cylinder subject to VIV at low mass-damping. Journal of Fluids and Structures 20, 483–503.

Menter, F.R., 1994. Two-equation eddy-viscosity turbulence models for engineering applications. AIAA Journal 32, 1598–1605.

Pantazopoulos, M.S., 1994. Vortex-induced vibration parameters: critical review. In: The 13th International Conference on Offshore Mechanics and Arctic Engineering, vol. 1, pp. 199–255.

Parkinson, G.V., 1974. Mathematical models of flow-induced vibrations of bluff bodies. In: Naudascher, E. (Ed.), Flow-Induced Structural Vibrations. Springer, Berlin, pp. 81–127.

Sarpkaya, T., 2004. A critical review of the intrinsic nature of vortex-induced vibrations. Journal of Fluids and Structures 19, 389–447.

Williamson, C.H.K., Govardhan, R., 2004. Vortex-induced vibrations. Annual Review of Fluid Mechanics 36, 413–455.

Williamson, C.H.K., Roshko, A., 1988. Vortex formation in the wake of an oscillating cylinder. Journal of Fluids and Structures 2, 355–381.